Articles in PresS. J Neurophysiol (June 3, 2015). doi:10.1152/jn.00980.2014

A temperature rise reduces trial-to-trial variability of locust auditory neuron responses

Monika J. B. Eberhard [1,*,+], Jan-Hendrik Schleimer[2,3,+], Susanne Schreiber[2,3], Bernhard Ronacher [1,3]

[1]Humboldt-Universität zu Berlin, Department of Biology, Behavioural Physiology Group, Invalidenstr. 43, 10115 Berlin, Germany
[2]Humboldt-Universität zu Berlin, Department of Biology, Institute for Theoretical Biology, Philippstr. 13, 10115 Berlin, Germany
[3]Bernstein Center for Computational Neuroscience Berlin, Philippstr. 13, 10115 Berlin, Germany

[+]these authors contributed equally

Running head: Temperature effects on locust auditory neurons

*Corresponding author: M. J. B. Eberhard
E-mail address: monika.eberhard@uni-greifswald.de
Present address: General Zoology and Zoological Systematics, Zoological Institute and Museum, Ernst-Moritz-Arndt-Universität Greifswald, Anklamer Str. 20, 17489 Greifswald, Germany
Phone: +49 3834 86 4286
Fax: +49 3834 86 4089

Abstract

The neurophysiology of ectothermic animals, such as insects, is affected by environmental temperature, as their body temperature fluctuates with ambient conditions. Changes in temperature alter properties of neurons and, consequently, have an impact on the processing of information. Nevertheless, nervous system function is often maintained over a broad temperature range, exhibiting a surprising robustness to variations in temperature. A special problem arises for acoustically communicating insects, as in these animals mate recognition and mate localization typically rely on the decoding of fast amplitude modulations in calling and courtship songs. In the auditory periphery, however, temporal resolution is constrained by intrinsic neuronal noise. Such noise predominantly arises from the stochasticity of ion channel gating and potentially impairs the processing of sensory signals. Based on intracellular recordings of locust auditory neurons, we show that intrinsic neuronal variability on the level of spikes is reduced with increasing temperature. We use a detailed mathematical model including stochastic ion channel gating to shed light on the underlying biophysical mechanisms in auditory receptor neurons: due to a redistribution of channel-induced current noise towards higher frequencies and specifics of the temperature dependence of the membrane impedance, membrane-potential noise is indeed reduced at higher temperatures. This finding holds under generic conditions and physiologically plausible assumptions on the temperature dependence of the channels' kinetics and peak conductances. We demonstrate that the identified mechanism also can explain the experimentally observed reduction of spike timing variability at higher temperatures.

Keywords – temperature, grasshopper, auditory neuron, intrinsic variability

INTRODUCTION

Because physiological processes strongly depend on temperature all aspects of animal life are affected by it. Chemical reaction rates typically exhibit Q_{10} values of 2.5-4 (Hoffmann 1995; Sanborn 2006), posing a challenge for ectothermic animals, such as insects, whose body temperatures are tightly coupled to the ambient temperature, and whose body functions usually have to be maintained over a broad temperature range of more than 20°C. For the nervous system of these animals, in particular, variations in temperature modulate fundamental properties of neurons

resulting in changes of spike rates, conduction velocity, or transmitter release (Burrows 1989; Franz and Ronacher 2002; Janssen 1992; Montgomery and MacDonald 1990; Robertson and Money 2012). As a consequence, the processing of sensory information as well as the coordination of movements should be affected. Nevertheless, several aspects of nervous system function of ectothermic animals have been found to show a relatively high level of robustness to temperature changes (eg. Caplan et al. 2014; Rinberg et al. 2013; Roemschied et al. 2014; Tang et al. 2010) in spite of various temperature-induced modifications in their elements – features that we are currently only beginning to understand.

In this study, we investigate the effect of temperature on sensory processing in the auditory periphery of locusts with a focus on the variability of spiking responses. Earlier investigations on locust auditory receptors and interneurons revealed an improved temporal resolution at higher temperatures (Franz and Ronacher 2002; Prinz and Ronacher 2002; Ronacher and Römer 1985). The neurophysiological data were complemented in behavioral tests: females of the grasshopper *Chorthippus biguttulus* are able to detect gaps as small as 1-2 ms in male songs at 35°C whereas at 23°C larger gaps are necessary to allow detection (Ronacher and Stumpner 1988; von Helversen 1972; von Helversen and von Helversen 1997). A better temporal resolution might be due to faster deterministic dynamics at higher temperatures, but also a reduction in neuronal noise might account for these findings. However, it is currently not known how intrinsic neuronal noise is affected by temperature changes in these animals.

In the case of auditory receptor neurons, i.e. the cells in the first layer of the feed-forward network that constitutes the locust auditory periphery, the largest noise source is cell-intrinsic (as these neurons do not receive synaptic inputs from other cells). It is not obvious, whether intrinsic noise is reduced at higher temperatures. On the contrary, in view of larger peak conductances and shorter activation time constants of ion channels, one may even expect increased noise levels at higher temperatures. We hence intracellularly recorded the responses of identified neurons, exposing them to two different temperatures. Interestingly, trial-to-trial spike variability was consistently reduced at the higher temperature. To understand the mechanisms underlying this reduction of spike jitter at warmer temperatures, we followed a

theoretical modeling approach: a detailed conductance-based model, including stochastic ion channels, was used to study the impact of temperature on spike rate and spike timing. Employing analytical techniques as well as model simulations we demonstrate that, indeed, voltage fluctuations at warmer temperatures are diminished in the vicinity of the firing threshold and, consequently, spike timing jitter is lowered. These findings hold under generic conditions and biophysically plausible assumptions on the temperature dependence of the channels' kinetics and peak conductances. The identified mechanism is likely to generalize beyond the locust receptor neurons.

MATERIALS AND METHODS

Experimental animals and electrophysiology

Experiments were performed on adult male and female *Locusta migratoria* L., obtained from a commercial supplier and held at room temperature (22-25°C). Head, legs, wings, and gut were removed and the animals fixed with wax, ventral side down onto a Peltier element (3 x 1.5 cm), which was attached to a holder. The thorax was opened dorsally and the metathoracic ganglion subsequently stabilized on a NiCr platform. The whole thorax was filled with locust saline solution (Pearson and Robertson 1981). Auditory receptors and interneurons were recorded intracellularly in the frontal auditory neuropil of the metathoracic ganglion using glass microelectrodes (borosilicate, GC100F-10; Harvard Apparatus, Edenbridge, UK) filled with a 3-5% solution of Lucifer yellow in 0.5 M LiCl. All electrophysiological experiments were conducted in a Faraday cage lined with foam prisms to minimize echoes. Neuronal responses were amplified (BRAMP-01; npi electronic GmbH, Tamm, Germany) and recorded by a data-acquisition board (BNC-2090A; National Instruments, Austin, TX, USA; sampling rate = 20 kHz).

The temperature of the preparation was controlled via the Peltier element connected to a 2V battery. A digital thermometer (GMH 3210, Greisinger electronic GmbH, Regenstauf, Germany) connected to a NiCr-Ni-thermoelement (GTF 300, Type K, Greisinger electronic GmbH, Regenstauf, Germany) was used to monitor and record temperature. The thermoelement was fixed between the Peltier element and the torso of the locust (underneath the ganglion), to prevent any disturbances of the neuronal recording. In most experiments, recordings were conducted first at 28-30°C, then the preparation was cooled down to 20-22°C and recordings were repeated for

the same neuron at the low temperature. Temperature changes at the Peltier element were completed in approximately 1 min. When the low temperature of the Peltier element had been reached, another 2 min were waited before the second recording started. Tissue temperature at electrophysiological recording sites was derived from temperature measurements at the Peltier element and calibrated according to a calibration curve, which had been created previously by measuring temperatures with three thermoelements; one at the Peltier element, one directly at the inner side of the tympanum, and one at the ganglion (see Eberhard et al. 2014; Roemschied et al. 2014). While in the majority of the measurements the preparations were cooled down, in four preparations the temperature change was reversed, starting with a low temperature; the direction of temperature change had no influence on measured Q_{10} values. After completion of the recordings Lucifer Yellow was injected into the recorded cell by applying hyperpolarizing current. The thoracic ganglia were then removed, fixed in 4% paraformaldehyde, dehydrated, and cleared in methyl salicylate. Stained cells were identified under a fluorescent microscope according to their characteristic morphology and physiology (Römer and Marquart 1984; Stumpner and Ronacher 1991). Altogether, we recorded from 13 receptor neurons, 25 local, and 24 ascending interneurons in 57 preparations (30 males, 27 females; in 5 preparations, two neurons were recorded). Parts of the data on receptor neurons have already been used in a different context in previous studies (Eberhard et al. 2014; Roemschied et al. 2014); to compare the temperature dependence of neurons of all three processing stages, we chose to re-investigate these data. Among local interneuron types, two segmental, one bisegmental and two different T-neurons were recorded; among ascending neurons, 7 different neuron types were recorded (see Table 1).

Stimulation

To obtain spike rate-intensity-functions, we used acoustic broad band stimuli (100 ms duration, 1-40 kHz bandwidth) repeated 5 times each at 8 intensities, rising from 32 to 88 dB SPL. Acoustic stimuli were stored digitally and delivered by a custom made program (LabView 7 Express, National Instruments, Austin, TX, USA). After a 100 kHz D/A conversion (BNC-2090A; National Instruments, Austin, TX, USA), the stimulus was routed through a computer-controlled attenuator (ATN-01M; npi electronic GmbH, Tamm, Germany) and an audio amplifier (Pioneer stereo amplifier

A-207R, Pioneer Electronics Inc., USA). Acoustic stimuli were unilaterally broadcast by speakers (D2905/970000; Scan-Speak, Videbæk, Denmark) located at ± 90° relative to the longitudinal axis of the preparation, at a distance of 30 cm from the animal. To control for directional sensitivity of a recorded neuron, the sound stimulation was first played from the left and then the right side or vice versa. Sound intensity was calibrated with a half inch microphone (type 4133; Brüel & Kjær, Nærum, Denmark) and a measuring amplifier (type 2209; Brüel & Kjær, Nærum, Denmark), positioned at the location of the preparation.

To test for changes in intrinsic variability for more complex stimuli, an additional set of stimuli was used in 15 recordings (see Fig. 5, Table 1,2): two model songs containing rectangular syllable envelopes, corresponding to mean syllable-pause lengths measured in *Chorthippus biguttulus* male songs at 30°C and 20°C (Block1 and Block2), part of a natural song recorded from a *Ch. biguttulus* male singing at 30°C (Origsong1), and the same natural song, expanded 1.7 times to correspond to a natural song at 20°C according to von Helversen (1972) (Origsong2). All stimulus envelopes were filled with a broadband noise of 1-40 kHz bandwidth. Song stimuli were presented 8 times each at 70 dB SPL, usually from the side (left or right) which showed a more sensitive reaction during presentation of the 100 ms stimuli. Note that locusts do not use calling songs for mate attraction, nevertheless, physiology and morphology of the auditory peripheral neurons are highly evolutionary conserved and homologous for *L. migratoria* and *Ch. biguttulus* (Neuhofer et al. 2008).

Data analysis

Spike times were extracted from the digitized recordings by applying a voltage threshold. Mean spike rates were calculated to obtain spike rate-intensity-functions per neuron, stimulation side, and temperature. From these curves, temperature coefficients (Q_{10} values) of the firing rate were determined: Rate changes with a 10° temperature shift can be expressed by the temperature coefficient Q_{10}:

$$Q_{10} = \left(\frac{X}{Y}\right)^{\frac{10}{(Tx-Ty)}}$$

where *X* is the rate at higher temperature (*Tx*) and *Y* is the rate at the lower temperature (*Ty*). A mean Q_{10} value was subsequently calculated for each neuron using only values at intensities eliciting spike rates above a threshold set at 50% of the maximum spike rate at the high temperature (see Fig. 1*A*). In addition, Q_{10}s for

first spike latencies, as well as action potential duration (width) and amplitude (height) were calculated for each recorded neuron. To determine Q_{10}s for action potential width and height, spontaneous action potentials recorded during trials (before the start of a stimulus) were detected, superimposed and the mean action potential shape was calculated. From this, height and width at half of the action potential amplitude were measured for each neuron and temperature (see Fig. 2*D*). Significance of differences between high and low temperature for the various characteristics measured was estimated using Wilcoxon matched pairs signed-rank tests, significance of differences in Q_{10} values of the three processing stages was calculated using Kruskal-Wallis tests, and post-hoc pairwise comparisons were performed using Wilcoxon rank-sum-tests, Bonferroni corrected.

To estimate intrinsic variability (trial-to-trial variability) of spike responses for each neuron and temperature, the pairwise metric distance between spike trains of the five repetitions per stimulus intensity (or between the eight repetitions of the model songs) was calculated according to van Rossum (2001). This metric yields an intuitive measure for the dissimilarity of spike trains, with large distance values indicating a high dissimilarity, that is, a large trial-to-trial variability. The van Rossum metric allows one to vary the temporal resolution of the comparison (via a resolution parameter τ). Equipped with very large τ values (> 200 ms), the metric largely ignores differences in the timing of spikes, and spike train dissimilarity depends only on spike count differences. With τ values of a few milliseconds, differences between the spike trains in both spike count and spike timing contribute to the dissimilarity. Previous investigations showed that the timing of spikes plays an important role for the encoding of acoustic signals at the level of thoracic neurons (Franz and Ronacher 2002; Stumpner et al. 1991). Therefore we used a temporal resolution of τ = 5 ms, which has been found to sufficiently encompass the coding properties of auditory neurons at different processing stages (Machens et al. 2003; Neuhofer et al. 2008; Wohlgemuth and Ronacher 2007). In addition, we also performed an analysis with τ varying between 2 and 1024 ms.

The van Rossum distance also depends on the number of spikes (Neuhofer et al. 2011). In order to compare distance values between hot and cold recordings, which may differ in spike rates, we standardized the distance values by the square root of the number of spikes elicited during the stimulus, to get a comparable average

distance (see Appendix 1). Subsequently, one mean distance value per neuron was calculated (mean distance over all intensities where a spike response was elicited, and a mean distance per neuron for all model songs together, respectively). For the model songs, the first 150 ms of each recording were omitted, to analyze the responses in the adapted state only.

All analyses were done using Matlab (R2012a, The MathWorks); graphs were edited in CorelDraw (X6, Corel Corporation).

Simulation

The modeling approach was focused on the first processing stage, the receptor neurons. A model capturing mechanotransduction as well as spike generation was implemented. It had previously been fitted to the locust mechano-receptors (Fisch et al. 2012) and replicates experimentally measured inter-spike interval distributions and serial correlations. For the transduction step, sound pressure waves evoke tympanal vibrations that in turn open and close mechano-sensitive ion channels (Appendix 2, Eq. (7)). The parameters of the tympanal oscillator are based on experiments using laser vibrometry (Schiolten et al. 1981). Biophysical details of the model are described in Appendix 2 (see Fig. 6*A*, for an equivalent circuit). All model parameters were taken from Fisch et al. (2012) and can be found in Table 4. Only the transduction parameters x_{base}, α and k_s were adapted to fit our measured rate intensity curves. The temperature coefficients were chosen from realistic ranges (Hille 2001): Q_{10} values of the peak conductances ranged in the interval [1,2], while the Q_{10} values of the ion channel kinetics are between [2.5,4]. The exact values were chosen such that in that the temperature effect on the firing rate was comparable to that of the measured responses (see Fig. 6B).

The model was simulated at 22°C and 32°C. For the stimuli, $s(t) = 20 \times 10^{I_{db}(t)/20} \xi_s(t)$, the broad band carrier that is typical for grasshopper songs was described by a Gaussian white noise process $\xi_s(t)$. Two classes of stimuli were applied: (*i*) A white noise carrier with constant amplitude $I_{db}(t) = \text{const.}$ given in dB SPL, to determine the rate-intensity curves (the result can be seen in Fig. 6*B*). (*ii*) The same time-dependent amplitude modulation, $I_{db}(t)$, as in the natural songs used in experiments (Fig. 6*C*). Stochastic ion channels were approximated by a diffusion equation instead of simulating the channel's Markov models (Linaro et al. 2011). More details can be found in Appendix 2. The simulated spike trains were analyzed in

the same way as the experimentally recorded ones. All simulations were performed in the `brian2` library (Stimberg et al. 2014). The temperature compensated response in the firing rate was achieved by selecting the Q_{10} values with a genetic algorithm (GA) from their given ranges. The GA objective was to minimize the mean squared-difference between hot and cold response, but was only allowed to choose realistic Q_{10} values from their respective intervals. For this the `deap` toolbox (Fortin et al. 2012), written in `python`, was used.

Analysis

To support the simulations and deepen the insight into the temperature effects on neuronal noise, formulas for the statistics of current and voltage fluctuations are provided in the following. Their detailed derivations can be found in in Appendix 3. In particular, the dependence on the temperature susceptibilities, Q_{10} values, is highlighted in the analysis. Peak conductances, ion channel kinetics and reversal potentials depend on temperature, T in Kelvin, as follows:

$$\begin{aligned} \mathrm{g_k(T)} &= \mathrm{g_k(T_{base})Q_{10}(g_k)}^{(\mathrm{T}-\mathrm{T_{base}})/10}, \\ \tilde{\tau}_{\mathrm{ki}}(\mathrm{T}) &= \tilde{\tau}_{\mathrm{ki}}(\mathrm{T_{base}})\mathrm{Q_{10}}(\tilde{\tau}_{\mathrm{i}})^{-(\mathrm{T}-\mathrm{T_{base}})/10}, \\ \mathrm{E_k(T)} &= \mathrm{E_k(T_{base})}\frac{\mathrm{T}}{\mathrm{T_{base}}}. \end{aligned} \quad (1)$$

Here, the index k stands for elements of the set, $\mathrm{k} \in \mathrm{K}$, of all channel types. In our model these were K={Na,K,M,R,L}, see Fig. 6*A*. The time constants $\tilde{\tau}_{\mathrm{ki}}$, together with the steady-state activation curves, which are not temperature dependent, describe the gating kinetics of channel k. Depending on the complexity of the underlying Markov model, there may be several time constants per channel involved.

To obtain a concise description of the total membrane current fluctuations in the receptor neuron model, it is approximated by a single colored, Gaussian noise process $\check{\eta}$, with correlation function $\mathrm{cov}(\Delta) = \check{\sigma}^2(\mathrm{v},\mathrm{T})\mathrm{e}^{-\|\Delta\|/\check{\tau}(\mathrm{v},\mathrm{T})}$. For a clamped voltage v and a fixed temperature T, the total noise power (*i.e.*, the integral over the noise spectrum) is given by (*cf.* Appendix 3)

$$\check{\sigma}^2(\mathrm{v},\mathrm{T}) = \sum_{\mathrm{k}\in\mathrm{K}} \quad \sum_{\mathrm{i}=1}^{\mathrm{M_k}-1} \quad \sigma_{\mathrm{ki}}{}^2(\mathrm{v})\mathrm{g_k}{}^2(\mathrm{T})(\mathrm{E_k(T)}-\mathrm{v})^2. \quad (2)$$

The number of states in the channel's Markov model is denoted by $\mathrm{M_k}$. The noise variance σ_{ki}, associated with each channel state is defined in Linaro et al. (2011) and depends only on the steady-state activation curves, and hence not on temperature. With this approximation the temperature influences the total noise power only through

the temperature susceptibilities of the peak conductances, $g_k(T)$, and the reversal potentials, $E_k(T)$. The effect on the reversal potentials is not substantial (~3%). The $Q_{10}(g_k)$ values are similar to that of aquatic diffusion and hence small compared to those of the reaction rates. In total, $\breve{\sigma}$ has a weak temperature dependence. In contrast, the time constant of the equivalent noise process $\breve{\eta}$, is given by

(3) $$\breve{\tau}(v,T) = \frac{\breve{\sigma}^2(v,T)}{\sum_{k\in K} \sum_{i=1}^{M_k-1} g_k{}^2(T)(E_k(T)-v)^2\sigma_{ki}{}^2(v)/\tau_{ki}(v,T)}.$$

Only in some case, like a simple two states channel or the linear chain in the model's K^+ channel, $\tau_{ki} \propto \tilde{\tau}_{ki}$, otherwise the expressions for the τ_{ki}'s may involve several of the original $\tilde{\tau}_{ki}$'s (*cf.* Linaro et al. 2011, Table 2). In general, the temperature scaling of $\breve{\tau}$ involves all Q_{10} values, including the strong temperature dependencies of the reaction kinetics. With this, the spectrum of the total noise current at a clamped command voltage v is then approximately a Lorentzian

(4) $$P_I(f) = \frac{\breve{\tau}(v,T)\breve{\sigma}^2(v,T)}{1+(f\breve{\tau}(v,T))^2}.$$

The quantitative link between spike jitter and subthreshold membrane voltage fluctuations is nontrivial (Alijani and Richardson 2011), yet voltage noise is a better predictor than unfiltered current fluctuations. Therefore, the current spectrum in Eq. (4) should be filtered by the membrane impedance to obtain the voltage fluctuations

(5) $$\sigma_V{}^2 = \int df\, Z(f)P_I(f).$$

The impedance for our model can be approximated by (*cf.* Appendix 3 for a justification)

(6) $$Z(f) \approx \frac{1}{\left(\frac{1\partial I_f}{c\partial V}\right)^2 + f^2}.$$

Note that the steady state value of $\partial I_f / \partial V$, again, only depends on the Q_{10} parameters of the peak conductances, $g_c(T)$, and the reversal potentials, $E_c(T)$. Consequently, the impedance is affected by temperature to a lesser degree, as can be inspected in Fig. 7*B*.

RESULTS

The first three processing stages of the auditory pathway form a hierarchically organized feed-forward network (in the metathoracic ganglion) and comprise receptor

neurons, thoracic local interneurons, and ascending interneurons, respectively (Clemens et al. 2012; Stumpner and Ronacher 1991; Stumpner et al. 1991; Vogel and Ronacher 2007). First, we characterized effects of temperature on response characteristics of neurons across all three layers. To this end, each cell was recorded at two different temperatures (at approximately 20°C and 30°C).

Temperature effects on basic parameters of neuronal responses

In all 62 recorded neurons spike rate increased with higher temperature (Fig. 1, Table 1). The general shape of the spike rate-intensity-functions did not change with temperature (i.e. saturating or unimodal curve – Fig. 1), nor was the basic spiking pattern of cells (phasic versus tonic response) affected. On average, the temperature dependence of the spike rate was smallest in receptor neurons (mean Q_{10} of 1.38 ± 0.19, median: 1.33). For local and ascending interneurons the temperature effect was more pronounced (Fig. 1D; mean: 2.45 ± 1.48 (median: 1.88), and 1.96 ± 0.91 (median: 1.68), respectively), see also Table 1.

Temperature changes affected action potential shape and first spike latencies (Fig. 2). At all three processing stages, neurons exhibited a significant decrease in action potential width (Fig. 2*E,H*) and latency with increased temperature (Fig. 2*F,I*), whereas spike amplitudes showed no consistent changes (Fig. 2*D,G*). Q_{10} values for action potential height and width did not significantly differ between neurons at the three processing stages (Kruskal-Wallis test, AP height: $\chi^2 = 2.33$, $P = 0.31$, AP width: $\chi^2 = 1.31$, $P = 0.52$).

Temperature effects on intrinsic neuronal variability

Timing of spikes is thought to contribute to the neuronal representation of fast amplitude modulations in grasshopper acoustic communication signals (Machens et al. 2001; Wohlgemuth et al. 2011). Trial-to-trial variability of spiking responses can hence impair the processing of these vital signals.

We therefore quantified the trial-to-trial variability of responses using the spike train metric introduced by van Rossum (2001). The metric can be applied with different values of the time constant τ (which is a parameter to the metric), setting the timescale of spike train comparison (small τ emphasizing spike timing on short timescales, large τ shifting emphasis rather to spike count than spike timing). Across cells from all processing stages of the peripheral network, spike train distances were

significantly larger at the lower temperature, provided we used a high temporal resolution (τ = 5 ms; Fig. 3, Wilcoxon matched pairs signed rank tests). In other words, for both the short 100 ms acoustic stimuli (Fig. 3) and the longer model songs (Fig. 5*A-C*) spike timing variability was decreased at the warmer temperature.

For receptor neurons, in particular, this relation was observed across all values of τ used in the analysis (Fig. 4*A*). Hence, both the intrinsic variability of spike count as well as of spike timing was decreased at warmer temperatures. For low values of τ, local and ascending interneurons exhibited the same trend, i.e. the spike timing variability decreased at higher temperature (Fig. 4*B,C*). However, with larger τ values (above 32 ms) differences in variability between the cold and warm temperatures disappeared, indicating that at these processing stages spike count variability was less affected by a temperature change than spike timing variability.

These results are further supported by the data obtained with long song models (Fig. 5). With a focus on spike timing, using a τ = 5 ms, most neurons exhibited a larger intrinsic variability at the lower temperature (Fig. 5*A,C*). Similar as for the short acoustic stimuli, for small values of τ spike timing variability was on average larger at the low temperature whereas this effect disappeared or even reversed for larger τ values (Fig. 5*D-E*).

Modeling

To identify the mechanisms underlying the observed reduction in intrinsic variability at elevated temperatures, we turned to computational modeling. Temperature is known to increase the peak conductances of ion channels. One may hence surmise a rise in conductance noise and, consequently, in current noise. Yet, two additional factors come into play: also transition rates between channel states are expedited, and the translation of current changes into voltage is governed by the membrane impedance, whose temperature dependence is likely to further modify the temperature effect on voltage noise. To dissect the impact of temperature on noise fluctuations at the different levels of current noise, voltage noise, and spike timing jitter, we analyzed a previously published quantitative model of the receptor dynamics (Fig. 6*A*).

First, a temperature dependence was introduced to this model assuming Q_{10} values for peak conductances and reaction rates of the individual ion channels, see Eq. (1) (Table 3). Q10 parameters were chosen from realistic parameter ranges to obtain rate-intensity curves with a temperature dependence comparable to that observed in

the experimental data (Fig. 6*B*). For details on the chosen parameter set see Appendix 2. Next, model responses to natural song stimuli were obtained from simulations at two different temperatures (Fig. 6*C*). The analysis of spike variability in the model yielded the same relation as in the experimental recordings: spike train variability was reduced at the warmer temperature (compare Fig. 6*D* and Fig. 4*A*). An advantage of this approach is that the model allows for an explicit dissection of the underlying biophysical mechanisms, which we discuss in the following. For moderate firing rates, spike jitter depends on voltage fluctuations at threshold (Alijani and Richardson 2011). The reduction in spike jitter should, therefore, be accompanied by smaller voltage fluctuations at the warmer temperature. In order to understand how the current noise produced by the multitude of stochastic ion channels affects voltage fluctuations, the model's noise current spectrum and membrane impedance were obtained both through simulation and analytical techniques (see Eq. (4) and Appendix 3). While an increase in temperature entailed only moderate changes to the variance of the total membrane noise current, it redistributed the noise power in the current spectrum to higher frequencies (Fig. 7*A*). However, the membrane impedance, which “translates” current noise to voltage noise, was much less affected by temperature and exhibited low-pass filter characteristics with virtually identical cutoff frequencies at both temperatures (Fig. 7*B*). Combining these two facts yielded the explanation for the reduction of neuronal noise at warmer temperatures: The additional power at high frequencies of the current noise was not translated to voltage fluctuations, because the impedance values at these high frequencies were low (at both temperatures). In contrast, the reduction in low-frequency power of the current noise resulted in a lower contribution of these frequencies to voltage noise at the warm temperature so that overall voltage noise was reduced. Mathematically, the different behavior of total noise power and impedance cutoff in contrast to noise current cutoff can be understood from the formulas summarized in Materials and Methods; for a derivation see Appendix 3. From these expressions it is clear that only the noise cutoff frequency, $1/\check{\tau}(v,T)$, is influenced by the strong temperature susceptibilities of the reaction kinetics. In contrast, the total noise strength, i.e., the integral of the power spectrum, and membrane impedance depend on the Q_{10} values of the peak conductances only (Appendix 2, Eq. (2) and (3)). The stronger temperature dependence of the cutoff frequency is a direct consequence of the fact that kinetic Q_{10} values are usually

larger than the Q_{10} values of peak conductances. While the former Q_{10} are found to be around 2.5-4 (Hille 2001), the latter lie close to the Q_{10} of aquatic diffusion coefficients, i.e., << 2.

DISCUSSION

The most remarkable finding of this study is a decrease of the overall trial-to-trial variability of auditory neuron responses at higher temperatures (Figs. 3 and 5). Several other response characteristics important for neuronal signaling were influenced by temperature in a similar way as reported for other auditory neurons; for example action potential width and spike latencies decreased with rising temperature (Figs. 1 and 2, compare with Abrams and Pearson 1982; Coro et al. 1994; Fonseca and Correia 2007; Korsunovskaya and Zhantiev 2007). In view of the strong temperature influence on ion channels kinetics (Q_{10} ~ 2.5-4, Hille 2001), the observed decrease in spike jitter at first glance seemed counterintuitive.

Mathematical modeling explains the effect of temperature on noise

We searched for a mechanistic explanation of the observed variability reduction, by studying voltage fluctuations near threshold in a model introduced by Fisch et al. (2012). We demonstrated that increasing temperature redistributes current noise power to higher frequencies, which then are filtered out by the membrane impedance and hence contribute little to voltage variance (Fig. 7). Together this explains the voltage noise reduction at warmer temperatures. The change in the spectrum of the total noise current is also in accordance with the formulas given for single channel noise spectra (DeFelice 1981; O'Donnell and van Rossum 2014). Our analytical treatment revealed under which conditions of the ion channels' Q_{10} parameters the reduction in voltage noise found in the simulations will take place. The total current noise power as well as the impedance cutoff are affected by the typically small Q_{10} values of peak conductances, while the cutoff frequency of the noise spectrum depends on the much larger Q_{10} values of opening and closing reaction rates (Hille 2001), and consequently show a stronger increase with temperature. Based on numerical simulations voltage fluctuations near threshold have previously been described in conductance-based models, where a qualitatively similar trend for temperature change was observed (Steinmetz et al. 2000).

In addition, the model was stimulated with the naturalistic songs used in the measurements. The experimentally observed reduction in trial-to-trial variability was reproduced by the model. We hence established that the model not only complies with the experimental spike statistics in a constant stimulus paradigm at a single temperature (Fisch et al. 2012), but also agrees with data for naturalistic time-dependent song stimuli at different temperatures. Our analytic formulae can be applied to models containing arbitrary ion-channel combinations, in order to analyze their impact on the noise statistics. In future work, it will enable one to detect compensatory mechanisms between the large amount of existing ion channels with their different time scales and temperature susceptibilities. While it has been demonstrated experimentally that ion channels, like Kv1 potassium channels, have an impact on cortical spike variability (Higgs and Spain 2011), our quantitative understanding of how the potpourri of channels present in nerve membranes jointly impact the voltage fluctuations is still incomplete. The mathematical ansatz in Appendix 3 can support a more rigorous analysis in this direction.

Relevance of temperature and noise

The body temperature of grasshoppers is tightly coupled to the ambient temperature, and their body functions have to be maintained over a broad temperature range of more than 20°C. In particular, the neuronal processing of calling and courtship songs is crucial for the recognition and attraction of sexual partners and is strongly influenced by temperature (Bauer and von Helversen 1987; Ronacher and Stange 2013; von Helversen 1972; von Helversen 1979). The songs of many grasshopper species comprise fast amplitude modulations which constitute important signals for species recognition and sexual selection (Elsner 1974; Kriegbaum 1989; Ronacher and Römer 1985; Ronacher and Stumpner 1988; von Helversen 1979). Hence, elements of the auditory pathway should attain a high temporal resolution to allow for a robust evaluation of sexual signals – and spike train variability is detrimental for this task (Neuhofer et al. 2011; Ronacher 2014).

Grasshopper auditory receptor neurons encode the fine structure of amplitude modulations of sound stimuli in their instantaneous firing rate (Machens et al. 2001; Wohlgemuth et al. 2011). The lower intrinsic variability at warmer temperatures hence could allow for a better resolution of fine temporal details. This is supported by studies using a modulation transfer function paradigm that demonstrated an

increased temporal resolution of auditory receptor neurons at higher temperature (Franz and Ronacher 2002; Prinz and Ronacher 2002; Ronacher and Römer 1985). Indeed, grasshoppers tested in a behavioral gap detection paradigm were able to detect gaps as small as 2 ms at 30°C, whereas at 22°C the minimal detected gap width was approximately 4 ms (Ronacher and Stumpner 1988). Similar improvements of temporal resolution with increasing temperature have been found in the fly's visual system (Tatler et al. 2000; Warzecha et al. 1999).

In summary, an elevated temperature leads to a reduction of spike timing variability in the grasshopper auditory periphery, which can be explained by a net decrease in the impact of channel noise on membrane voltage. The mechanisms, characterized in the mathematical model, are likely to generalize and to apply to neurons beyond the specific system at hand. This study shows that in order to decipher the effect of temperature on neuronal computation and to understand principles that enable a robustness to temperature changes (Caplan 2014; Rinberg et al. 2013; Robertson and Money 2012; Roemschied et al. 2014), not only deterministic, but also stochastic mechanisms need to be taken into account. Further studies must reveal how the interplay of several different temperature mediated effects lead to the robust encoding of auditory signals, which is reflected in the behavior of grasshoppers that respond to acoustic signals within a large temperature range.

APPENDIX

Appendix 1: Normalization of the van Rossum metric

The original van Rossum metric (van Rossum 2001) is defined by $\tilde{d}^2 = \int ([y_1(t) - y_2(t)] * h(t))^2 dt$, in which two Dirac-spike trains are denoted as $y_{1,2}(t) = \sum_{k=1}^{N_{sp}^{(1,2)}} \delta(t - t_k^{(1,2)})$, with spikes occurring at times $t_k^{(1)}$ and $t_k^{(2)}$. The convolution operator is denoted by * and $h(t)$ is either an exponential kernel, $h(t) = H(t)\sqrt{2/\tau}\, e^{-t/\tau}$ (van Rossum 2001), or the synaptic α-function (Machens et al. 2003). H denotes Heaviside's step function: $H(t) = 1$ if $t > 0$ and $H(t) = 0$ if $t < 0$.

In the article, a normalized version of the van Rossum metric is used. The square of the original expression is divided by the spike count, N_{sp}, to obtain

$$d^2 = \frac{2\tilde{d}^2}{N_{sp}^{(1)} + N_{sp}^{(2)}} = \frac{2}{N_{sp}^{(1)} + N_{sp}^{(2)}} \int ([y_1(t) - y_2(t)] * h(t))^2 dt.$$

The motivation for the normalization is to obtain a measure by which cold and hot spike train variabilities can be put into perspective, even if the spike counts are different. Fig. 8 shows that the unnormalized van Rossum distance $\tilde{d}$ between two Poisson processes, indeed, scales with the square root of the mean spike count. The figure shows an example with $\tau = 2$, but note that the graph is independent of the time scale τ. The same scaling is found for two inhomogeneous Poisson processes with the same instantaneous rates and, generically, for all Poisson processes in the limit of small τ (Tomas and Sousa 2008).

Appendix 2: Auditory receptor model

The current balance equation for the voltage, $v(t)$, of a single compartment model of the auditory receptors in locusts, proposed in (Fisch et al. 2012), reads

$$c\dot{v} + I_{Na} + I_K + I_L + I_M + I_R = 0$$

It comprises the ionic currents $\mathrm{I_{Na}}$, $\mathrm{I_K}$ and $\mathrm{I_L}$, responsible for the spike generation, as well as an M-type adaptation current, $\mathrm{I_M}$, and the receptors' transduction current, $\mathrm{I_R}$. The membrane capacitance c is $1\mu\mathrm{F/cm^2}$. All parameter values can be found in Table 4.

The tympanal deflections, $\mathrm{x(t)}$, induced by an external sound pressure wave, $\mathrm{s(t) = 20 \times 10^{I_{db}(t)/20}\xi_s(t)}$, are described as a damped stochastic oscillation

(7) $\ddot{\mathrm{x}} + (2/\tau_\mathrm{d})\dot{\mathrm{x}} + {\omega_\mathrm{ty}}^2\,\mathrm{x} = \alpha \mathrm{s(t)} + \sigma_\mathrm{ty}\,\xi_\mathrm{x}(\mathrm{t})$.

The input $\mathrm{s(t)}$ is imbibed with a gain factor α, that was determined from stroboscopic measurements (Breckow and Sippel 1985; Fisch et al. 2012). The thermal fluctuations ξ_x of the tympanum are a white noise process with variance ${\sigma_\mathrm{ty}}^2 = (4\alpha \mathrm{k_B T})/(\tau_\mathrm{d} \mathrm{B})$, where B is the vibrating area of the tympanum and $\mathrm{k_B}$ is Bolzmann's constant. The eigenfrequency and the damping time constant of the tympanum are ω_ty and τ_d respectively, have previously been determined by laser vibrometry (Eberhard et al. 2014; Schiolten et al. 1981).

The tympanal vibrations are transduced into a receptor current $\mathrm{I_R = G_R(t)(v - E_R)}$ by an unidentified receptor, possibly of the TRP family as in *Drosophila* (Zhang et al. 2013). The receptor channel is assumed to have two states, follows first order kinetics, and has an activation function described by Howard and Hudspeth (1988) and Hudspeth et al. (2000)

$$\mathrm{z_\infty(x)} = \frac{1}{1 + \exp(-\frac{\mathrm{k_s}}{\mathrm{k_B T}}(\mathrm{x} - \mathrm{x_{base}}))} + \frac{1}{1 + \exp(\frac{\mathrm{k_s}}{\mathrm{k_B T}}(\mathrm{x} + \mathrm{x_{base}}))}.$$

The spring constant $\mathrm{k_s}$, the half-maximum of the mechano-transducer $\mathrm{x_{base}}$, and the tympanal gain α, were adapted to fit the recorded rate-intensity curves, *cf.* Fig. 6*B*. All other channels follow typical Markov state models from the literature (Fisch et al. 2012).

In total, there are three different noise sources in the equations above. First of all, thermal noise from the tympanum (ξ_x). Secondly, the input which consists of a modulated white noise carrier (ξ_s). And thirdly, noise from stochastic ion channel gating, discussed next.

Stochastic ion channels

Instead of simulating the master equations for the stochastic ion channels, one (Linaro et al. 2011) of several (Fox and Lu 1994; Goldwyn et al. 2011; Orio and Soudry 2012) diffusion approximations available in the literature are used. This casts the problem into a stochastic differential equation (SDE) which facilitates the following mathematical analysis.

As an example, take the receptor channel from above. It is modeled as a two-state (open-closed) Markov model (Fisch et al. 2012). The gating variable $\mathrm{G_R}$ that approximate the two-state Markov dynamics, can be split into a deterministic z and a stochastic η_z part, $\mathrm{G_R} = \overline{\mathrm{g}}_\mathrm{R}(\mathrm{z} + \eta_\mathrm{z})$. According to Linaro et al. (2011) the governing equations read

$$\begin{aligned} \tau_\mathrm{z}(\mathrm{T})\dot{\mathrm{z}} &= (\mathrm{z}_\infty(\mathrm{x}) - \mathrm{z}), \\ \tau_\mathrm{z}(\mathrm{T})\dot{\eta}_\mathrm{z} &= -\eta_\mathrm{z} + \sqrt{2\tau_\mathrm{z}}\sigma_\mathrm{z}\,\xi_\mathrm{z}(\mathrm{t}). \end{aligned} \tag{8}$$

In the two state case, the noise variance given by Fox and Lu (1994) is valid. It reads $\sigma_\mathrm{z}^2 = \tau_\mathrm{z}(\mathrm{z}_\infty(\mathrm{x})(1-\mathrm{z}) + (1-\mathrm{z}_\infty(\mathrm{x}))\mathrm{z})$, which in the steady state becomes $\sigma_\mathrm{z}^2(\mathrm{x}) = {\mathrm{N_R}}^{-1}\mathrm{z}_\infty(\mathrm{x})(1-\mathrm{z}_\infty(\mathrm{x}))$.

For fixed tympanal position x, Eq. (8) is an Ornstein-Uhlenbeck (OU) process. The temperature dependence of $\tau_\mathrm{z}(\mathrm{T})$ follows Eq. (1).

Ion channels with $\mathrm{n} > 2$-dimensional state space require as many OU processes to represent the correlation structure as there are reactions. The voltage dependent activation curves and time constants of these OU processes are obtained from an eigendecomposition of the infinitesimal transition matrices of the Markov models (Tuckwell 1989). For the Na^+ and K^+ channels used here, they are given in Linaro et al. (2011). The M-type adaptation conductance is modeled as a two-state channel like the receptor.

Appendix 3: Model analysis

The complete rate-intensity curve of a nonlinear and stochastic membrane is not analytically tractable. The calculation of the statistical properties of the firing rate can be divided into three mathematical problems: (*i*) well below threshold, the firing rate is given as an escape process, with Poisson statistics; (*ii*) well above threshold the system exhibits a stochastic limit cycle, with inverse Gaussian statistics; (*iii*), an intermediate regime where both descriptions break. The intermediate regime is important for amplitude coding, as it spans the largest dynamic range. The spike fluctuations in that regime are related to voltage noise (O'Donnell and van Rossum 2014). Hence, the following calculation focuses on deriving the voltage noise close to threshold under varying temperature.

Simplification of the transduction

To start with, the transduction dynamics is simplified. This step reduces the simulation time, because the integration of the tympanal oscillations of the full system would render the SDE system stiff. Furthermore, the transduction channel can now be treated as just one more channel that contributes to the total voltage noise.

Note from the model parameters in Table 4 that the difference in time scale between the eigen-frequency of the tympanum and the time constant of the receptor channel, $\tau_z > 2\pi/\omega_{ty}$, prevents a locking of spikes to the tympanal oscillations, in accordance with experimental observations (Sippel and Breckow 1983). Moreover, this difference in time scale allows for an adiabatic elimination (Titulaer 1980) of the fast variables x and $\dot{x}$, leaving us with analytic expressions for mean and variance of the receptor gating variable, z, as a function of the input intensity I_{db}. This procedure formalizes the intuition that, because the receptor kinetics are slower than the tympanal dynamics, they are only affected by the average statistics of the deflections. Thus, it suffices to take the equilibrium distribution, $p_\infty(x; I_{db})$, of the tympanum's vibrations to average over Eq. (8). Since Eq. (7) is a noisy harmonic oscillator, the marginal equilibrium distribution of the tympanal excursion, x, is given by

(9) $$p_\infty(x; I_{db}) = (\sqrt{2\pi}\sigma_x)^{-1}\exp\left(-\frac{x^2}{2\sigma_x^2}\right).$$

The dependence on the input I_{db} is mediated by the variance

$$\sigma_x^2 = ((\alpha \cdot 20 \times 10^{I_{db}/20})^2 + {\sigma_{ty}}^2)\tau_d/4{\omega_{ty}}^2,$$

i.e., a louder sound produces a larger deviation in the tympanal deflections. The theoretical distributions and the histograms obtained from numerical simulations at two input intensities are illustrated in Fig 9*A*.

Applying the adiabatic elimination procedure (Titulaer 1980) to the drift and diffusion parts of Eq. (8) requires calculation of the averaged steady-state activation curve

(10) $$\tilde{z}_\infty(I_{db}) = \int_{-\infty}^{\infty} dx\ p_\infty(x; I_{db})\, z_\infty(x) \approx 1 - \frac{\tanh(k_s x_{base}/(2k_B T))}{\left(1+\left(\frac{k_s\sigma_x}{k_B T}\mathrm{sech}(\frac{k_s x_{base}}{2k_B T})\right)^2\right)^{\frac{1}{2}}}.$$

To obtain the analytical approximations above, the activation function z_∞ is approximated by a Gaussian, so that the integrals can be evaluated using Laplace's method (MacKay 2003). In addition, the averaged diffusion coefficient is needed. So, *mutatis mutandis*, $z_\infty(1 - z_\infty)$ can be approximated by one minus a Gaussian, which yields

(11) $$\tilde{\sigma}_z^2(I_{db}) = \int_{-\infty}^{\infty} dx\ p_\infty(x; I_{db})\, \sigma_z^2(x) \approx \frac{\frac{\beta {x_{base}}^2}{2e^{2(1-\beta\sigma_x^2)}}\left(\frac{1}{4} - \frac{1}{\left(1+e^{2k_s x_{base}/k_B T}\right)^2}\right)}{N_R\sqrt{1-\beta\sigma_x^2}},$$

where

$$\beta = -\frac{k_s^2(5 + 40e^{2k_s x_{base}/k_B T} + 18e^{4k_s x_{base}/k_B T} + e^{8k_s x_{base}/k_B T})}{2(3 + 4e^{2k_s x_{base}/k_B T} + e^{4k_s x_{base}/k_B T})^2 k_B^2 T^2}.$$

The reduced gating SDE for the two state receptor channel then has the following structure $\tau_z(T)\,\dot{z} = z_\infty(I_{db}) - z + \sqrt{2\tau_z}\sigma_z(I_{db})\,\xi_z(t)$.

The symbol $\xi_z(t)$ denotes a zero-mean, white noise process. In this approximation, for any fixed mean input I_{db} and temperature T, the transduction gating variable will be Gaussian. This effectively eliminates the state space dimensions corresponding to the noisy tympanal oscillations. The accuracy of this approximation can be inspected in Fig. 9*B* and *C*.

Noise current spectrum

The currents in the balance equation for the voltage dynamics can be separated into deterministic, $I_d(v)$, and stochastic, $I_f(v)$, parts

$$C\dot{v} + I_d(v) + I_f(v) = 0.$$

The drift contains the deterministic model components. Near the fixed point it reads

$$I_d(v) = \bar{g}_{Na}(T)m_\infty^3(v)h_\infty(v)(v - E_{Na}(T)) + \bar{g}_K(T)n_\infty^4(v)(v - E_K(T)) \\ +\bar{g}_L(T)(v - E_L(T)) + \bar{g}_M(T)w(v - E_M(T)) + \bar{g}_R(T)\tilde{z}_\infty(I_{db})(v - E_R(T)),$$

while the stochastic part is

$I_f(v) = \bar{g}_{Na}(T)(v - E_{Na}(T))\sum_{k=1}^{M_{Na}-1}\eta_k + \bar{g}_K(T)(v - E_K(T))\sum_{j=1}^{M_K-1}\eta_j + \bar{g}_M(T)(v -$
$E_M(T))\eta_w + \bar{g}_R(T)(v - E_R(T))\eta_z.$

Here, M_c is the number of states of the $c \in \{Na, K, M, R\}$-channel. The noise processes are exponentially correlated OU processes

$$\tau_k(v,T)\dot{\eta}_k = -\eta_k + \sqrt{2\tau_k(v,T)}\,\sigma_k(v)\,\xi_k,$$

where all ξ_k's denote zero-mean, white noise processes. The analytic expressions for the voltage dependent variances $\sigma_k(v)$ and time constants, $\tau_k(v,T)$ are determined from the eigenvectors and eigenvalues of the infinitesimal transition matrix of the Markov chains respectively (Linaro et al. 2011; Tuckwell 1989). The expression for the variance of the receptor channel was derived in Eq. (11).

As a next step, the fluctuating part is approximated by a single OU process, fitted to reproduce the correlation time of the superposition of OU processes in I_f. The auto-correlation of I_f under voltage clamp and in steady state is

$\langle I_f(t)I_f(t+\Delta)\rangle = \bar{g}_{Na}{}^2(v - E_{Na})^2\sum_{k=1}^{M_{Na}-1}\sigma_k{}^2(v)e^{-\|\Delta\|/\tau_k(v)}$

$+\bar{g}_K{}^2(v - E_K)^2\sum_{j=1}^{M_K-1}\sigma_j(v)^2e^{-\|\Delta\|/\tau_j(v)} + \bar{g}_M{}^2(v - E_K)^2\sigma_M(v)^2e^{-\|\Delta\|/\tau_M(v)} + \bar{g}_R{}^2(v -$

$E_K)^2\tilde{\sigma}_R^2(I_{db})e^{-\|\Delta\|/\tau_z}.$

This is approximated by a single OU process, $\check{\eta}$ with correlation $\check{\sigma}^2(v,T)e^{-\|\Delta\|/\check{\tau}(v,T)}$, by Taylor expanding both the single OU and the sum of OUs. Based on this expression both $\check{\sigma}$ and $\check{\tau}$ can be identifed (see Eqs. (2) and (3)).

Hence, the power spectrum of the total noise current is the Fourier transform of the correlation function at a clamped command voltage v is then approximately a Lorentzian $P_i(f) = \frac{\check{\tau}(v)\check{\sigma}^2(v)}{1+(f\check{\tau}(v))^2}$.

Importantly, the total variance of the membrane current, $\check{\sigma}^2$, is only affected by the Q_{10} values of the peak conductances, which are relatively small (<2.0). On the other hand, the cutoff frequency, $\check{\tau}^{-1}$, of the total membrane noise current depends on the Q_{10} parameters of reaction kinetics, which are comparatively large (>2.0). This leads to the redistribution of noise power to higher frequencies shown in Fig. 7*A*.

Membrane impedance

The subthreshold impedance filter can be derived by linearization around the resting potential. The poles and zeros of the impedance filter are then related to the eigenvalues of system's Jacobian matrix. In the case of a type one neuron this simplifies and the impedance is a lowpass filter approximately given by

$$Z(f) \approx \frac{1}{((\frac{1}{c}\frac{\partial I_f}{\partial V})^2 + f^2)}.$$

Note that the steady state value of $\partial I_f / \partial V$ only depends on the Q_{10} parameters of the peak conductances. Consequently the impedance it affected by temperature to a lesser degree, as can be inspected in Fig. 7*B*.

Together with the conclusion of the previous section this means: If all $Q_{10}(g_c)$ values are well below 2 and the $Q_{10}(\tau_i)$ values are sufficiently large, voltage noise fluctuations are reduced when temperature increases (*cf.*: Fig. 7*C*).

ACKNOWLEDGEMENTS

We thank J. Clemens for providing help to MJBE concerning Matlab programming, and F. Roemschied for providing a tool to calculate mean action potential shape.

GRANTS

This work was funded by the German Research Council (DFG: SFB 618, grant to BR and SS, RO547/12-1) and the Federal Ministry of Education and Research, Germany (01GQ1001A, 01GQ0901, 01GQ0972, grants to BR and SS).

DISCLOSURE

No conflicts of interest, financial or otherwise, are declared by the authors.

REFERENCES

Abrams TW, and Pearson KG. Effects of temperature on identified central neurons that control jumping in the grasshopper. *J Neurosci* 2: 1538-1553, 1982.

Alijani AK, and Richardson MJE. Rate response of neurons subject to fast or frozen noise: From stochastic and homogeneous to deterministic and heterogeneous populations. *Physical Review E* 84: 011919, 2011.

Bauer M, and von Helversen O. Separate localization of sound recognizing and sound producing neural mechanisms in a grasshopper. *J Comp Physiol A* 161: 95-101, 1987.

Breckow J, and Sippel M. Mechanics of the transduction of sound in the tympanal organ of adults and larvae of locusts. *J Comp Physiol A* 157: 619-629, 1985.

Burrows M. Effects of temperature on a central synapse between identified motor neurons in the locust. *J Comp Physiol A* 165: 687-695, 1989.

Caplan JS, Williams AH, and Marder E. Many parameter sets in a multicompartment model oscillator are robust to temperature perturbations. *J Neurosci* 34: 4963-4975, 2014.

Clemens J, Wohlgemuth S, and Ronacher B. Nonlinear computations underlying temporal and population sparseness in the auditory system of the grasshopper. *J Neurosci* 32: 10053-10062, 2012.

Coro F, Pérez M, and Machado A. Effects of temperature on a moth auditory receptor. *J Comp Physiol A* 174: 517-525, 1994.

DeFelice LJ. *Introduction to membrane noise*. Plenum Press, 1981.

Eberhard MB, Gordon S, Windmill JC, and Ronacher B. Temperature effects on the tympanal membrane and auditory receptor neurons in the locust. *J Comp Physiol* 1-11, 2014.

Elsner N. Neuroethology of sound production in gomphocerine grasshoppers (Orthoptera: Acrididae). *J Comp Physiol* 88: 67-102, 1974.

Fisch K, Schwalger T, Lindner B, Herz AVM, and Benda J. Channel Noise from Both Slow Adaptation Currents and Fast Currents Is Required to Explain Spike-Response Variability in a Sensory Neuron. *J Neurosci* 32: 17332-17344, 2012.

Fonseca PJ, and Correia T. Effects of temperature on tuning of the auditory pathway in the cicada *Tettigetta josei* (Hemiptera, Tibicinidae). *J Exp Biol* 210: 1834-1845, 2007.

Fortin F-A, De Rainville F-M, Gardner Gardner M-A, Parizeau M, and Gagné C. DEAP: evolutionary algorithms made easy. *J Mach Learn Res* 13: 2171-2175, 2012.

Fox RF, and Lu Y-n. Emergent collective behavior in large numbers of globally coupled independently stochastic ion channels. *Physical Review E* 49: 3421-3431, 1994.

Franz AF, and Ronacher BR. Temperature dependence of temporal resolution in an insect nervous system. *J Comp Physiol A* 188: 261-271, 2002.

Goldwyn JH, Imennov NS, Famulare M, and Shea-Brown E. Stochastic differential equation models for ion channel noise in Hodgkin-Huxley neurons. *Physical Review E* 83: 041908, 2011.**Higgs MH, and Spain WJ**. Kv1 channels control spike threshold dynamics and spike timing in cortical pyramidal neurones. *J Physiol* 589: 5125-5142, 2011.

Hille B. *Ionic channels of excitable membranes*. Sunderland, MA: Sinauer, 2001.

Hoffmann KH. Stoffwechsel. In: *Physiologie der Insekten*, edited by Gewecke M. Stuttgart, Jena, New York: Gustav Fischer Verlag, 1995, p. 1-65.

Howard J, and Hudspeth A. Compliance of the hair bundle associated with gating of mechanoelectrical transduction channels in the Bullfrog's saccular hair cell. *Neuron* 1: 189-199, 1988.

Hudspeth AJ, Choe Y, Mehta AD, and Martin P. Putting ion channels to work: Mechanoelectrical transduction, adaptation, and amplification by hair cells. *PNAS* 97: 11765-11772, 2000.

Janssen R. Thermal influences on nervous system function. *Neurosci Biobehav Rev* 16: 399-413, 1992.

Korsunovskaya O, and Zhantiev R. Effect of temperature on auditory receptor functions in crickets (Orthoptera, Tettigoniodea). *J Evol Biochem Phys* 43: 327-334, 2007.

Kriegbaum H. Female choice in the grasshopper Chorthippus biguttulus. *Naturwissenschaften* 76: 81-82, 1989.

Linaro D, Storace M, and Giugliano M. Accurate and Fast Simulation of Channel Noise in Conductance-Based Model Neurons by Diffusion Approximation. *PLoS Comput Biol* 7: e1001102, 2011.
Machens CK, Schütze H, Franz A, Kolesnikova O, Stemmler MB, Ronacher B, and Herz AVM. Single auditory neurons rapidly discriminate conspecific communication signals. *Nature Neuroscience* 6: 341-342, 2003.
Machens CK, Stemmler MB, Prinz P, Krahe R, Ronacher B, and Herz AVM. Representation of Acoustic Communication Signals by Insect Auditory Receptor Neurons. *J Neurosci* 21: 3215-3227, 2001.
MacKay DJ. Information theory, inference, and learning algorithms [Online]. Citeseer. http://citeseerx.ist.psu.edu/viewdoc/download?doi=10.1.1.228.899&rep=rep1&type=pdf [17 Feb. 2015].
Montgomery JC, and MacDonald JA. Effects of temperature on nervous system: implications for behavioral performance. *Am J Physiol* 259: 191-196, 1990.
Neuhofer D, Stemmler M, and Ronacher B. Neuronal precision and the limits for acoustic signal recognition in a small neuronal network. *J Comp Physiol A* 197: 251-265, 2011.
Neuhofer D, Wohlgemuth S, Stumpner A, and Ronacher B. Evolutionarily conserved coding properties of auditory neurons across grasshopper species. *Proc R Soc Lond B Biol Sci* 275: 1965-1974, 2008.
O'Donnell C, and van Rossum MCW. Systematic analysis of the contributions of stochastic voltage gated channels to neuronal noise. *Frontiers in Computational Neuroscience* 8: 2014.
Orio P, and Soudry D. Simple, Fast and Accurate Implementation of the Diffusion Approximation Algorithm for Stochastic Ion Channels with Multiple States. *PLoS ONE* 7: e36670, 2012.
Pearson KG, and Robertson RM. Interneurons coactivating hindleg flexor and extensor motoneurons in the locust. *J Comp Physiol A* 144: 391-400, 1981.
Prinz PP, and Ronacher BR. Temporal modulation transfer functions in auditory receptor fibres of the locust (*Locusta migratoria* L.). *J Comp Physiol A* 188: 577-587, 2002.
Rinberg A, Taylor AL, and Marder E. The Effects of Temperature on the Stability of a Neuronal Oscillator. *PLoS Comput Biol* 9: e1002857, 2013.
Robertson RM, and Money TGA. Temperature and neuronal circuit function: compensation, tuning and tolerance. *Curr Opin Neurobiol* 22: 724-734, 2012.
Roemschied FA, Eberhard MJB, Schleimer J-H, Ronacher B, and Schreiber S. Cell-intrinsic mechanisms of temperature compensation in a grasshopper sensory receptor neuron. *eLife* 3: e02078, 2014.
Römer H, and Marquart V. Morphology and physiology of auditory interneurons in the metathoracic ganglion of the locust. *J Comp Physiol A* 155: 249-262, 1984.
Ronacher B. Processing of species-specific signals in the auditory pathway of grasshoppers. In: *Insect hearing and acoustic communication* edited by Hedwig B. Berlin: Springer, 2014, p. 185-204
Ronacher B, and Römer H. Spike synchronization of tympanic receptor fibres in a grasshopper (*Chorthippus biguttulus* L., Acrididae). *J Comp Physiol* 157: 631-642, 1985.
Ronacher B, and Stange N. Processing of acoustic signals in grasshoppers – A neuroethological approach towards female choice. *J Physiology-Paris* 107: 41-50, 2013.
Ronacher B, and Stumpner A. Filtering of behaviourally relevant temporal parameters of a grasshopper's song by an auditory interneuron. *J Comp Physiol* 163: 517-523, 1988.
Sanborn AF. Acoustic signals and temperature. In: *Insect Sounds and Communication*, edited by Drosopoulos S, and Claridge MF. Boca Raton, London, New York: Taylor & Francis Group, 2006, p. 111-125.
Schiolten P, Larsen O N, and Michelsen, A. Mechanical time resolution in some insect ears. *J Comp Physiol* 143: 289-295, 1981.
Sippel M, and Breckow J. Non-linear analysis of the transmission of signals in the auditory system of the migratory locust Locusta migratorta. *Biol Cybern* 46: 197-205, 1983.
Steinmetz PN, Manwani A, Koch C, London M, and Segev I. Subthreshold voltage noise due to channel fluctuations in active neuronal membranes. *J Comput Neurosci* 9: 133-148, 2000.

Stimberg M, Goodman DFM, Benichoux V, and Brette R. Equation-oriented specification of neural models for simulations. *Front. Neuroinform.* 8, 2014.
Stumpner A, and Ronacher B. Auditory interneurones in the metathoracic ganglion of the grasshopper *Chorthippus biguttulus*: I. Morphological and physiological characterization. *J Exp Biol* 158: 391-410, 1991.
Stumpner A, Ronacher B, and von Helversen O. Auditory interneurones in the metathoracic ganglion of the grasshopper *Chorthippus biguttulus*: II. Processing of temporal patterns of the song of the male. *J Exp Biol* 158: 411-430, 1991.
Tang LS, Goeritz ML, Caplan JS, Taylor AL, Fisek M, and Marder E. Precise temperature compensation of phase in a rhythmic motor pattern. *PLoS Biol* 8: e1000469, 2010.
Tatler B, O'Carroll DC, and Laughlin SB. Temperature and the temporal resolving power of fly photoreceptors. *J Comp Physiol A* 186: 399-407, 2000.
Titulaer UM. The Chapman-Enskog procedure as a form of degenerate perturbation theory. *Physica A: Statistical Mechanics and its Applications* 100: 234-250, 1980.
Tomas P, and Sousa L. Statistical analysis of a spike train distance in Poisson Models. *Signal Processing Letters, IEEE* 15: 357-360, 2008.
Tuckwell HC. *Stochastic processes in the neurosciences*. Philadelphia: Society for Industrial and Applied Mathematics, 1989.
van Rossum MCW. A Novel Spike Distance. *Neural Comput* 13: 751-763, 2001.
Vogel A, and Ronacher B. Neural correlations increase between consecutive processing levels in the auditory system of Locusts. *J Neurophysiol* 97: 3376-3385, 2007.
von Helversen D. Gesang des Männchens und Lautschema des Weibchens bei der Feldheuschrecke *Chorthippus biguttulus* (Orthoptera, Acrididae). *J Comp Physiol A* 81: 381-422, 1972.
von Helversen D, and von Helversen O. Recognition of sex in the acoustic communication of the grasshopper *Chorthippus biguttulus* (Orthoptera, Acrididae). *J Comp Physiol A* 180: 373-386, 1997.
von Helversen O. Angeborenes Erkennen akustischer Schlüsselreize. *Verh dt Zool Ges* 72: 42-59, 1979.
Warzecha A, Horstmann W, and Egelhaaf M. Temperature-dependence of neuronal performance in the motion pathway of the blowfly *Calliphora erythrocephala*. *J Exp Biol* 202: 3161-3170, 1999.
Wohlgemuth S, and Ronacher B. Auditory Discrimination of Amplitude Modulations Based on Metric Distances of Spike Trains. *J Neurophysiol* 97: 3082-3092, 2007.
Wohlgemuth S, Vogel A, and Ronacher B. Encoding of amplitude modulations by auditory neurons of the locust: influence of modulation frequency, rise time, and modulation depth. *J Comp Physiol A* 197: 61-74, 2011.
Zhang W, Yan Z, Jan LY, and Jan YN. Sound response mediated by the TRP channels NOMPC, NANCHUNG, and INACTIVE in chordotonal organs of Drosophila larvae. *Proceedings of the National Academy of Sciences* 110: 13612-13617, 2013.

Figure legends

Fig. 1. Examples of spike rate-intensity-functions obtained from locust auditory neurons at two different temperatures. *A:* local interneuron SN1, *B:* ascending interneuron AN1, *C:* ascending interneuron AN3 (for spike rate-intensity-functions of receptor neurons see Eberhard et al. 2014; Roemschied et al. 2014). *D:* Boxplots of Q_{10} values of spike rate of all recorded cells showing means (circles), medians (thick lines), 25/75 percentiles (boxes), 1.5 Inter-Quartile-Range (whiskers) and outliers (+);

horizontal bars show pairwise comparisons (Wilcoxon signed-rank-tests, Bonferroni corrected). *** – $P < 0.001$, *NS* – not significant.

Fig. 2. Effect of temperature on characteristics of auditory neurons. *A-C* show voltage traces of a receptor (*A*), a local (*B*), and an ascending interneuron (*C*) at high and low temperatures in response to a 100 ms auditory stimulus (56 dB SPL). *D-F:* Boxplots of Q_{10} values for action potential height (*D*), width (*E*), and first spike latency (*F*). *G-I:* Pairwise comparisons of action potential height (*G*), width (*H*) and latency time (*I*) at the two temperatures (hot & cold). *P* values shown here were calculated using a Wilcoxon matched pairs signed rank test for each group. *NS* – not significant.

Fig. 3. *A-C*: Spike-raster-plots of example neurons recorded at high and low temperatures using short broad-band noise stimuli at different intensities (indicated at the sides of the raster-plots, dB SPL). Five repetitions per stimulus intensity are shown for a receptor neuron (*A*), local interneuron BSN1 (*B*) and ascending interneuron AN3 (*C*). *D*: Variability values (metric distance in arbitrary units) calculated using the metric according to van Rossum, $\tau = 5$ ms. Variability values at hot temperature minus those at cold temperature and *P* values from Wilcoxon matched pairs signed rank tests for all recorded neurons of the three processing stages. *E-F*: Pairwise comparisons of distance values at the hot vs. cold temperature for receptors (*E*), local (*F*) and ascending (*G*) interneurons (IN).

Fig. 4. *A*: Variability values at cold temperature subtracted from variability values at hot temperature for receptors, local and ascending interneurons for different values of the metric's temporal resolution parameter τ. At large τ values only spike count differences contribute to the metric value, while for small τ also differences in spike timing become relevant. Grey boxplots show a significant difference from zero (i.e. a significant change of intrinsic variability with temperature), while white boxes are not significantly different from zero (i.e. no change of variability with temperature).

Fig. 5. Variability values resulting from applying the van Rossum-metric to spike trains of neurons recorded during stimulation with the 4 model songs. *A:* Variability values at hot temperatures minus values at cold temperatures for $\tau = 5$ ms. Grey diamonds mark the mean variability calculated over all 4 model songs, grey circles

879 indicate mean variability differences obtained with the short 100ms stimuli. *B*:
880 Example spike-raster-plots of a receptor neuron and ascending interneuron AN3,
881 recorded at high and low temperatures; shown are eight repetitions of the same
882 stimulus (Origsong1). *C:* Pairwise comparisons of mean variability values for $\tau = 5$
883 ms. *D,E:* Mean change (variability hot – variability cold) of intrinsic variability with
884 temperature, using different values of τ. For each neuron, an average variability value
885 for all 4 model songs was calculated.
886
887 Fig. 6. *A*: Equivalent circuit of the auditory receptor model. Tympanal vibrations are
888 transduced by receptor channels (E_R). Other channels included in the model are
889 spike generating Na-, and K channels, leak channels (L) as well as adaptation
890 channels (M). *B*: Rate-intensity curves of the model at 22ºC and 32ºC. Also included
891 in *B* is a plot of action potential width at two temperatures as derived from the model.
892 *C*: Spike response for natural, time-dependent stimuli at 22ºC (cold) and 32ºC (hot).
893 *D*: Average difference in spike train-metric (hot minus cold) for different values of τ. In
894 all cases the distance value decreased at the high temperature, indicating both a
895 decrease in spike-time jitter and spike count variability. Model and simulation
896 parameters can be found in Appendix 2.

897 Fig. 7. *A*: Power spectral density of the total current noise at 22ºC (light grey, dashed
898 line) and 32ºC (dark grey, solid line) in voltage clamp condition (command voltage is -
899 67mV). All stochastic ion-channels, including the transduction contribute to the
900 fluctuations, but to different degrees. The weighted sum in Eq. (2) and (3) describes
901 this behavior. Dots show estimated spectra, while lines are the theoretical prediction
902 from Eq. (4). The main effect of the temperature increase is a shift of noise power to
903 the high frequency range. Vertical line denotes the cutoff frequency of the impedance
904 filter. *B*: Temperature dependence of the membrane impedance filter in the
905 subthreshold dynamical regime. Simulations (dots) are compared with the
906 approximative, analytical formula (lines, Eq. (6)). *C*: Membrane voltage fluctuations
907 near the resting state are reduced in the model neuron with higher temperature. The
908 observed temperature dependence is a combination of the redistribution in noise
909 power towards higher frequencies in (*A*) and the relative temperature invariance of
910 the cutoff frequency of the membrane impedance in (*B*). Parameters as in Fig. 9.

Fig. 8. Unnormalized spike train metric, $\tilde{d}$, for two independent Poisson processes with increasing number of spikes. Solid line shows the theoretical square-root scaling of the spike metric and dots are simulated Poisson processes. N_{sp} – spike count.

Fig. 9. Comparison between theory and simulation for the receptor model with transduction. *A*: Probability distribution of tympanal deflections (as indicated in the schematics below) in response to white noise stimuli at two different sound intensities (I_{db} = 40 dB SPL and I_{db} = 50 dB SPL). Solid lines represent the Gaussian distribution from Eq. (9). *B*: Probability distributions of the conductance fluctuations of the receptor channels (depicted in the schematics - R) induced by the two inputs. Solid lines represent theoretical predictions based on the quasi-static averaging, Eqs. (10) and (11). *C*: Comparison of the mean and variance of the receptor gate z as a function of the sound input. Black dots depict the mean open probability and errorbars denote the standard deviation. The dark grey line shows the theoretical curve from Eq. (10) and the grey shaded area the standard deviation, see Eq. (11). *E:* Sketch of the rate-intensity curve. The intensity and fluctuations of the transduction current are translated into a spike frequency by voltage dependent ion channels (depicted in the schematics *D*), resulting in a rate-intensity curve. The two output frequencies for I_{db} = 40, 50 dB are marked by vertical lines. T=22°C, all other parameters as given in the Tables 3 and 4.

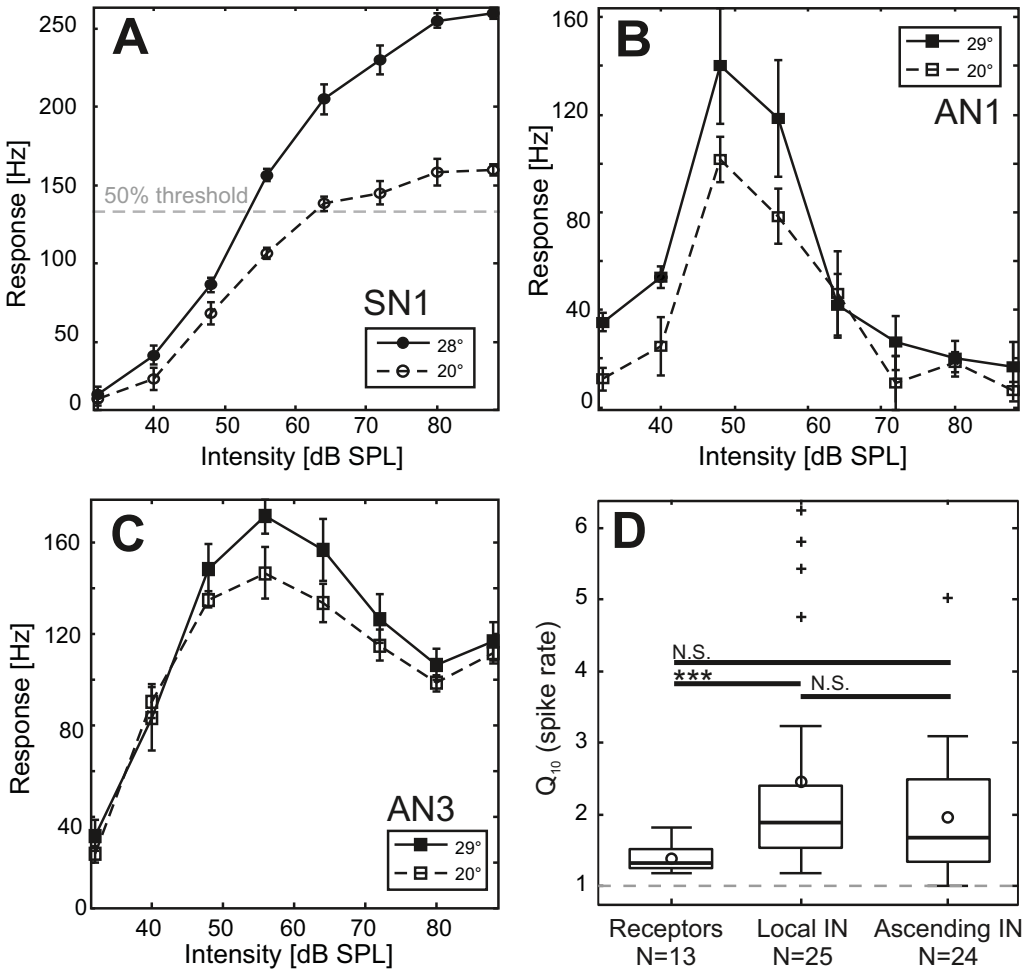
A
Response [Hz]
250
200
150
100
50
0
50% threshold
SN1
28°
20°
40
50
60
70
80
Intensity [dB SPL]
B
160
120
80
40
0
29°
20°
AN1
C
AN3
D
Q_{10} (spike rate)
6
5
4
3
2
1
N.S.
***
N.S.
Receptors
N=13
Local IN
N=25
Ascending IN
N=24

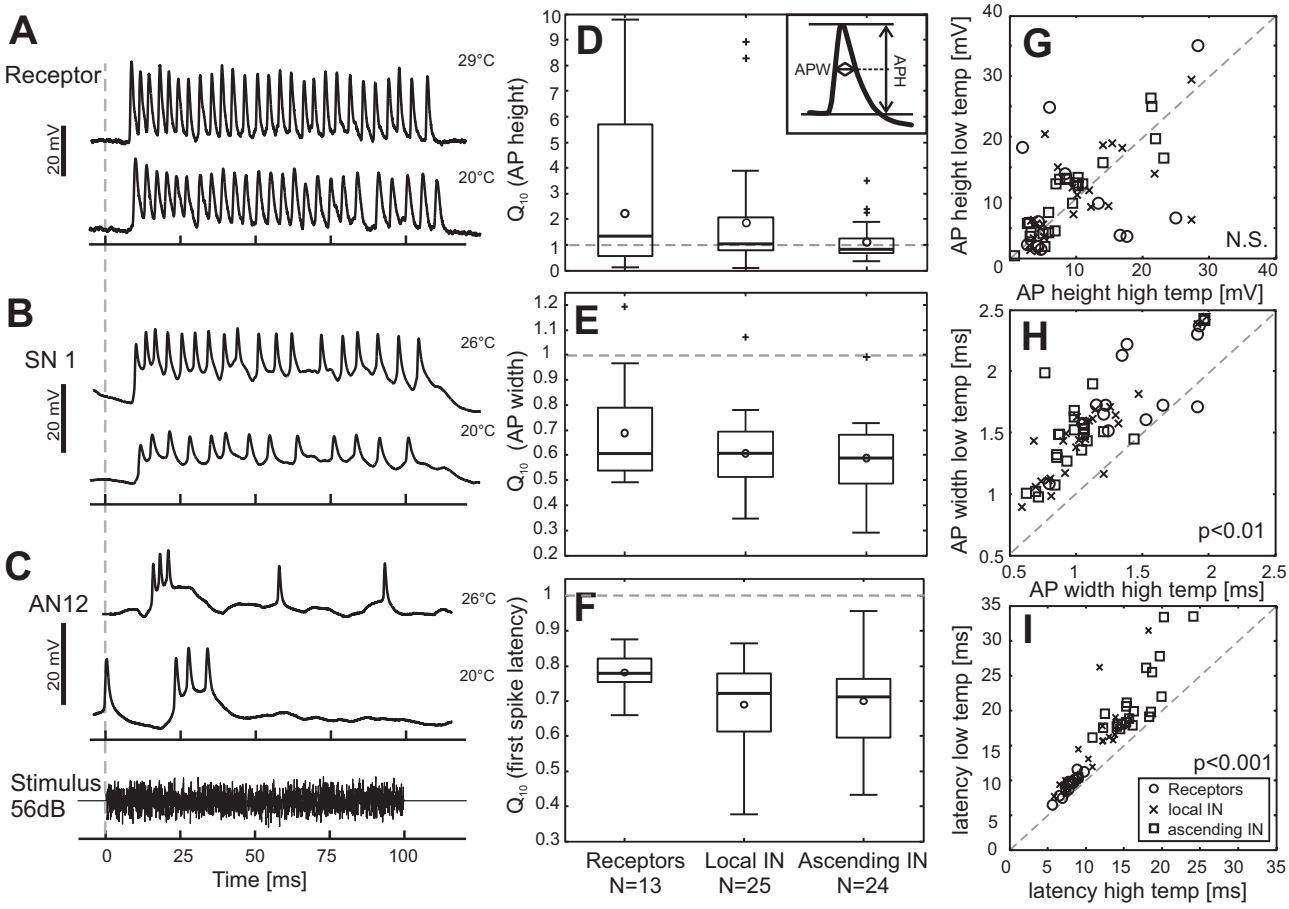
A
Receptor
29°C
20°C
20 mV
B
SN 1
26°C
20°C
20 mV
C
AN12
26°C
20°C
20 mV
Stimulus
56dB
0
25
50
75
100
Time [ms]
D
APW
APH
Q10 (AP height)
E
Q10 (AP width)
F
Q10 (first spike latency)
Receptors
N=13
Local IN
N=25
Ascending IN
N=24
G
AP height low temp [mV]
AP height high temp [mV]
N.S.
H
AP width low temp [ms]
AP width high temp [ms]
p<0.01
I
latency low temp [ms]
latency high temp [ms]
p<0.001
Receptors
local IN
ascending IN

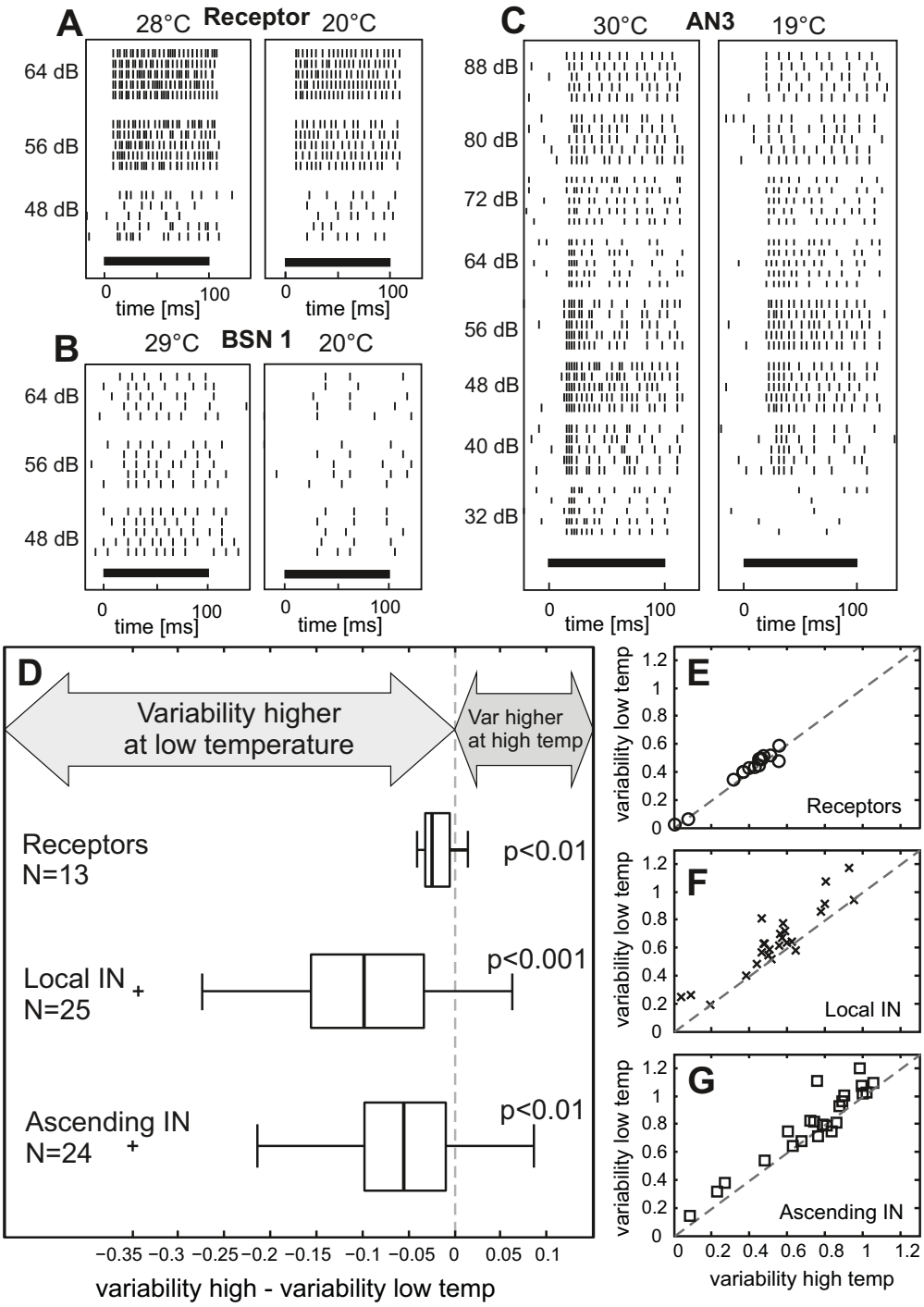
A
28°C
Receptor
20°C
64 dB
56 dB
48 dB
0
100
time [ms]
B
29°C
BSN 1
20°C
C
30°C
AN3
19°C
88 dB
80 dB
72 dB
64 dB
56 dB
48 dB
40 dB
32 dB
D
Variability higher
at low temperature
Var higher
at high temp
Receptors
N=13
p<0.01
Local IN
N=25
p<0.001
Ascending IN
N=24
p<0.01
−0.35 −0.3 −0.25 −0.2 −0.15 −0.1 −0.05 0 0.05 0.1
variability high - variability low temp
E
Receptors
F
Local IN
G
Ascending IN
variability low temp
variability high temp
0 0.2 0.4 0.6 0.8 1 1.2

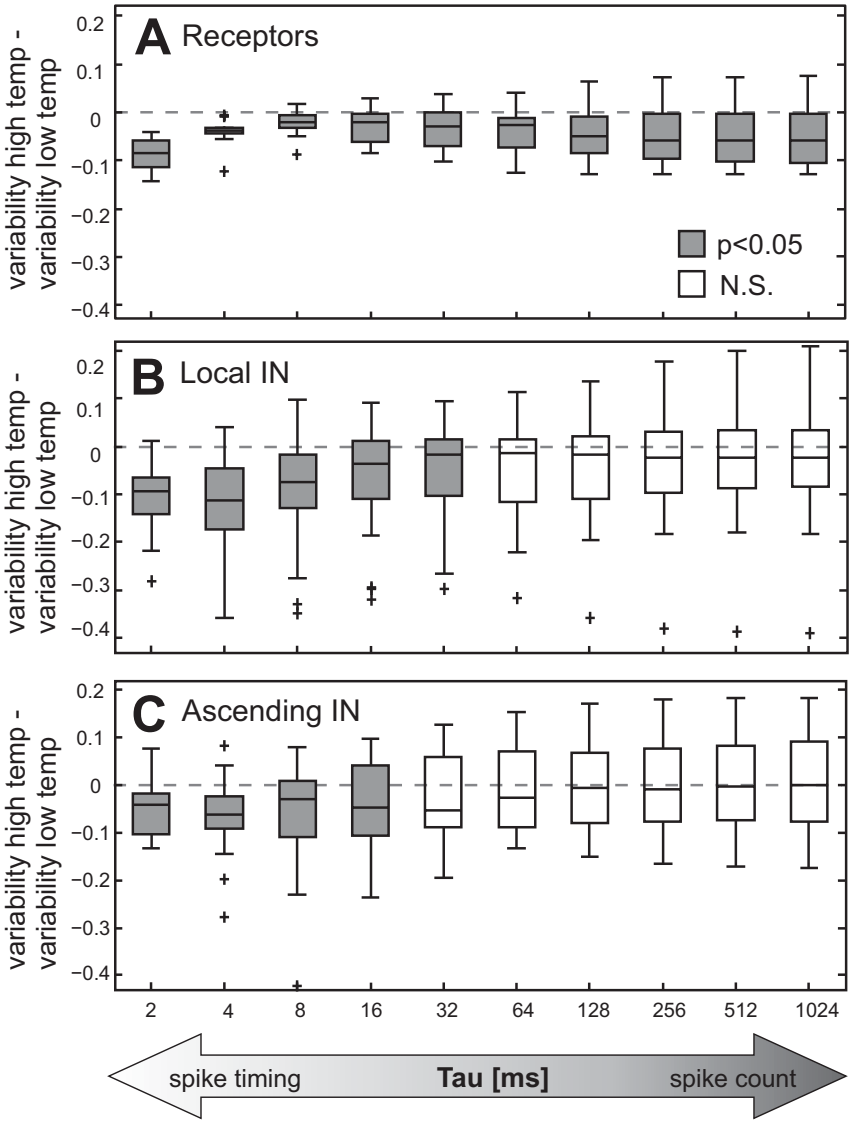
A Receptors
B Local IN
C Ascending IN
variability high temp - variability low temp
p<0.05
N.S.
0.2
0.1
0
−0.1
−0.2
−0.3
−0.4
2
4
8
16
32
64
128
256
512
1024
spike timing
Tau [ms]
spike count

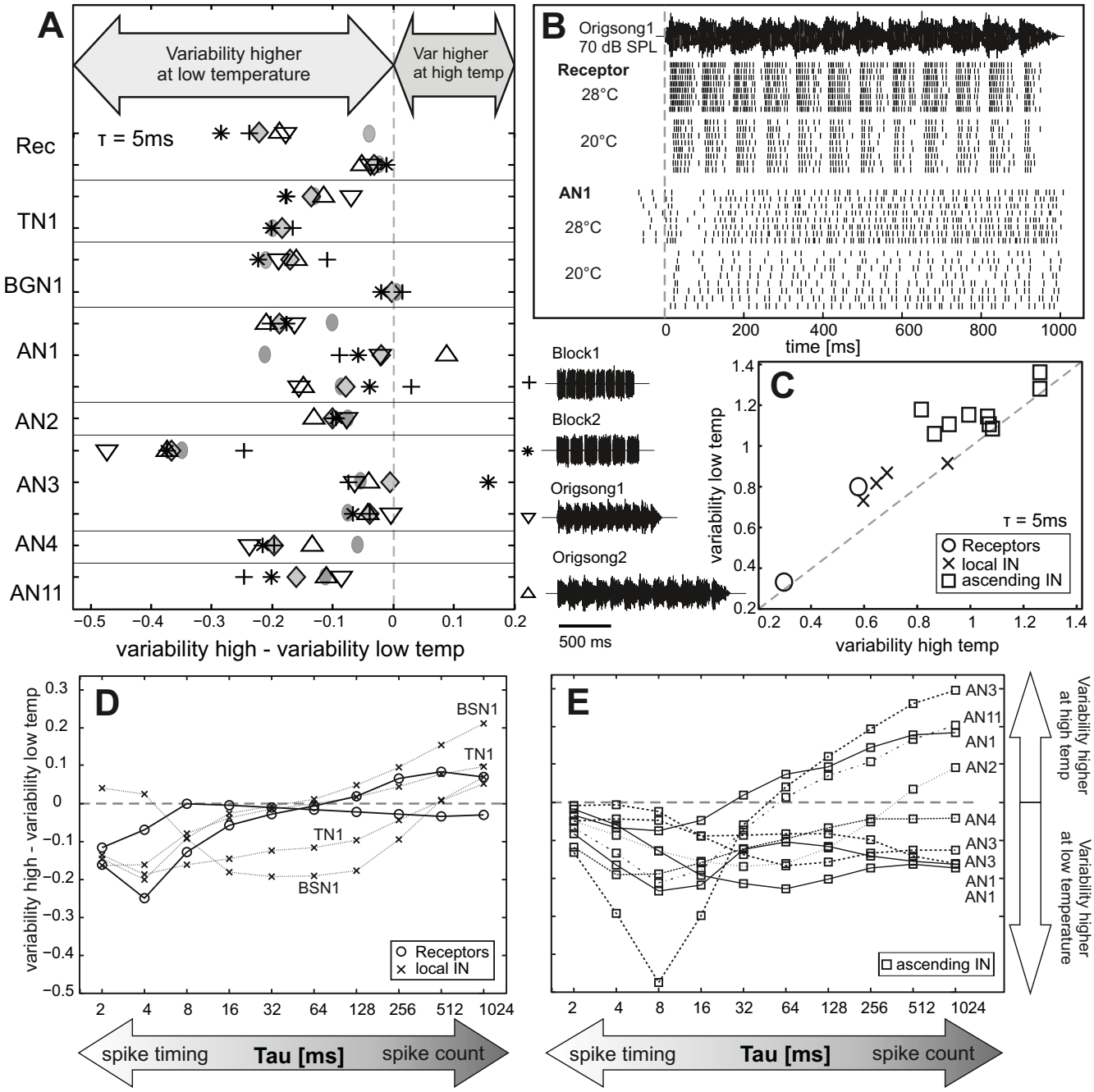
A
Variability higher at low temperature
Var higher at high temp
τ = 5ms
Rec
TN1
BGN1
AN1
AN2
AN3
AN4
AN11
variability high - variability low temp
B
Origsong1
70 dB SPL
Receptor
28°C
20°C
AN1
28°C
20°C
time [ms]
Block1
Block2
Origsong1
Origsong2
500 ms
C
variability low temp
variability high temp
τ = 5ms
Receptors
local IN
ascending IN
D
variability high - variability low temp
BSN1
TN1
TN1
BSN1
Receptors
local IN
spike timing
Tau [ms]
spike count
E
AN3
AN11
AN1
AN2
AN4
AN3
AN3
AN1
AN1
ascending IN
Variability higher at high temp
Variability higher at low temperature
spike timing
Tau [ms]
spike count

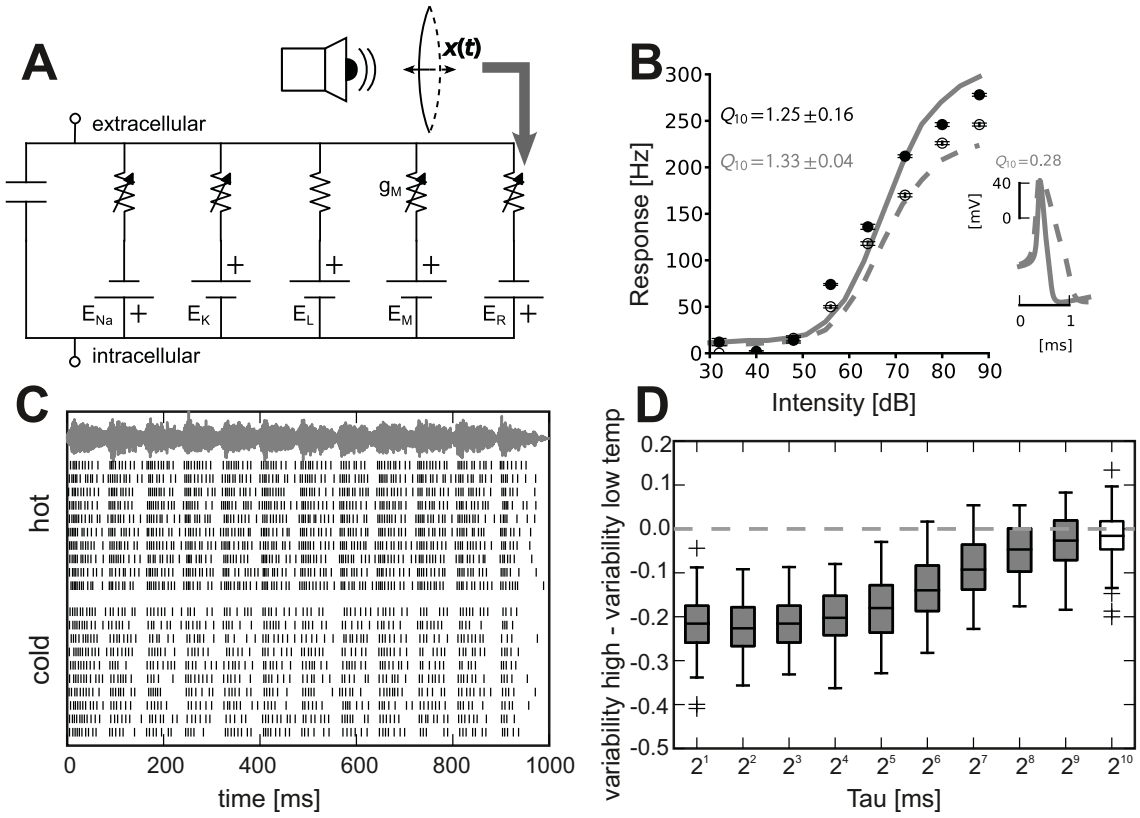
A
x(t)
extracellular
g_M
E_{Na}
E_K
E_L
E_M
E_R
intracellular
B
Q_{10}=1.25±0.16
Q_{10}=1.33±0.04
Q_{10}=0.28
Response [Hz]
Intensity [dB]
[mV]
[ms]
C
hot
cold
time [ms]
D
variability high - variability low temp
Tau [ms]

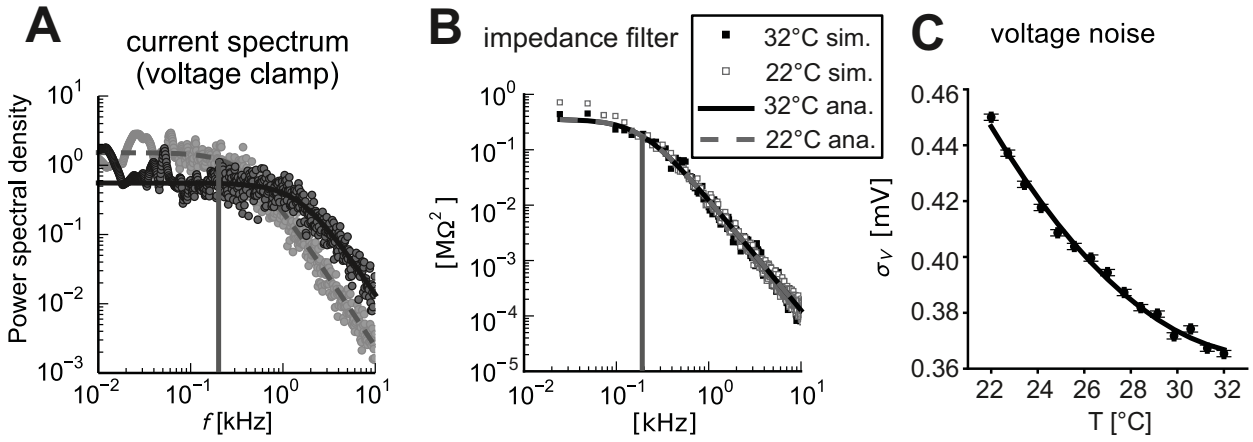
A
current spectrum
(voltage clamp)
Power spectral density
f [kHz]
B
impedance filter
32°C sim.
22°C sim.
32°C ana.
22°C ana.
[MΩ²]
[kHz]
C
voltage noise
σV [mV]
T [°C]

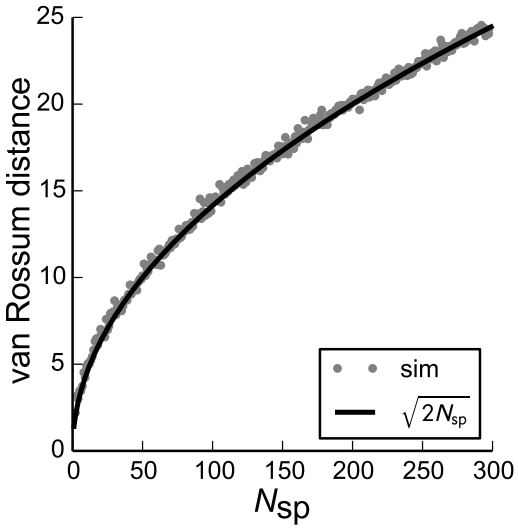
van Rossum distance
25
20
15
10
5
0
0
50
100
150
200
250
300
N_{sp}
sim
$\sqrt{2N_{sp}}$

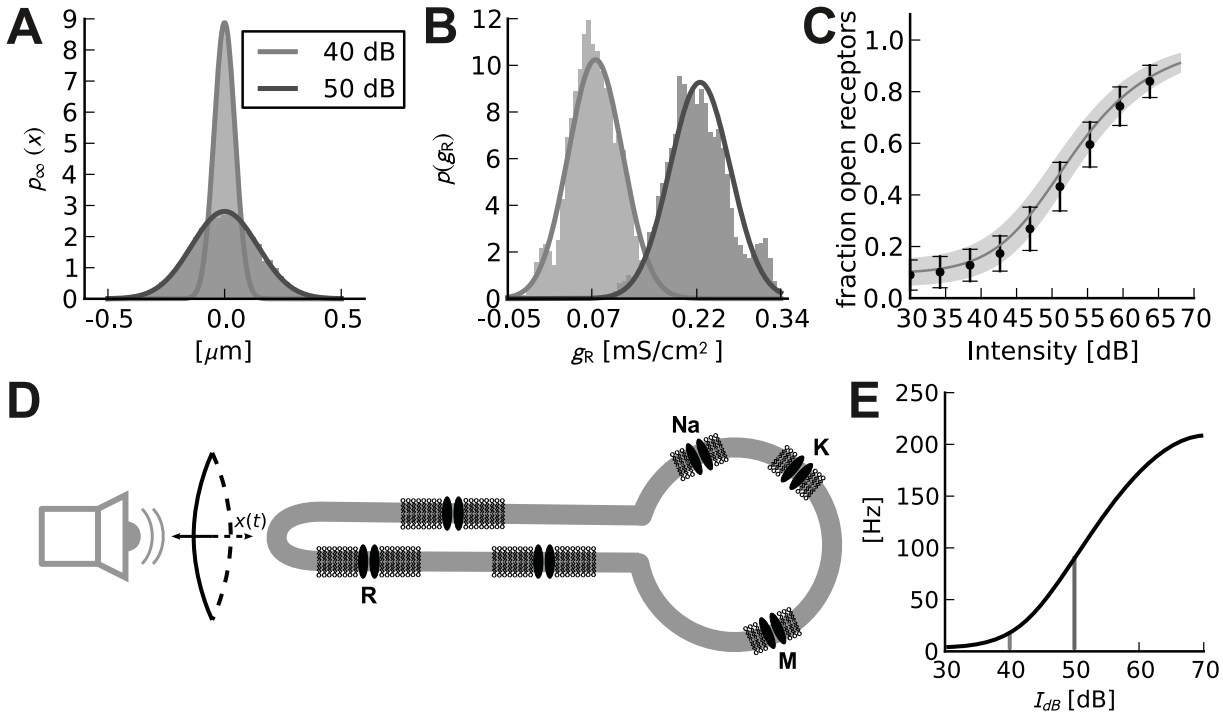
A
B
C
D
E
40 dB
50 dB
$p_\infty(x)$
[μm]
$p(g_R)$
g_R [mS/cm^2]
fraction open receptors
Intensity [dB]
x(t)
Na
K
R
M
[Hz]
I_{dB} [dB]

Table 1. *Temperature dependence of locust auditory neurons*

neuron type	neuron name	number of recordings	model songs tested	mean Q_{10} ± SD	median Q_{10}
Receptors	-	13	2	1.38 ± 0.19	1.33
Local Interneurons	SN1	6		1.81 ± 0.54	1.71
	SN4	1		2.40	2.40
	BSN1	11	2	3.14 ± 1.98	2.02
	TN1	6	2	1.69 ± 0.27	1.65
	TN4	1		3.24	3.24
Ascending Interneurons	AN1	9	3	2.22 ± 1.20	1.74
	AN2	2	1	2.09 ± 1.10	2.09
	AN3	7	3	1.91 ± 0.76	1.72
	AN4	1	1	1.51	1.51
	AN11	2	1	1.74 ± 0.09	1.74
	AN12	2		1.30 ± 0.41	1.30
	AN15	1		-	-

Number and names of recorded neurons, together with mean ± SD and median Q_{10} for spike rate for each neuron type. For AN15 no Q_{10} (spike rate) could be calculated, as the neuron was inhibited for the duration of the stimulus. Each neuron was recorded at two different temperatures. Nomenclature after Römer and Marquart (1984) and Stumpner and Ronacher (1991).

Table 2. *Model songs used in electrophysiological recordings*

Model song	Number of syllables	Syllable length [ms]	Pause length [ms]	Total length [ms]
Block1	8	77	17	752
Block2	6	110	24	804
Origsong1	12	71.1	17.8	1020
Origsong 2	12	121.9	30.2	1700

Note that for the original songs, mean syllable and pause lengths are given. See also Fig. 5.

Table 3. *Q_{10} parameters of peak conductances, activation and inactivation kinetics*

Parameter	Q_{10}	Parameter	Q_{10}
g_{Na}	2.00	Na act.	2.50
g_K	1.10	Na inact.	2.50
g_M	2.00	K act.	2.50
g_R	1.10	M act.	3.74
gL	1.10	R act.	2.50

Table 4. *Model parameters (Param)*

Param	value	Param	value
N_M	600	τ_h	$\frac{\left(e^{-\frac{v}{5}-\frac{27}{5}}+1\right)}{0.128\left(e^{-\frac{v}{5}-\frac{27}{5}}+1\right)e^{-\frac{v}{18}-\frac{25}{9}}+4}$ ms
N_K	40000		
N_R	10	τ_n	$\frac{\left(-e^{-\frac{v}{5}-\frac{52}{5}}+1\right)}{0.032v-0.5\left(e^{-\frac{v}{5}-\frac{52}{5}}-1\right)e^{-\frac{v}{40}-\frac{57}{40}}+1.664}$ ms
N_{Na}	40000		
k_B	13.8 μm^2 fg/(ms^2 K)	τ_m	$\frac{\left(e^{-\frac{v}{4}-\frac{27}{2}}-1\right)\left(e^{\frac{v}{5}+\frac{27}{5}}-1\right)}{(0.28v+7.56)\left(e^{-\frac{v}{4}-\frac{27}{2}}-1\right)-(0.32v+17.28)\left(e^{\frac{v}{5}+\frac{27}{5}}-1\right)}$ ms
x_{base}	0.26 μm		
g_K	80 mS/cm^2	h_∞	$\frac{0.128\left(e^{-\frac{v}{5}-\frac{27}{5}}+1\right)e^{-\frac{v}{18}-\frac{25}{9}}}{0.128\left(e^{-\frac{v}{5}-\frac{27}{5}}+1\right)e^{-\frac{v}{18}-\frac{25}{9}}+4}$
g_R	0.5 mS/cm^2		
g_{Na}	100 mS/cm^2	w_∞	$\frac{1}{e^{-\frac{v}{5}-4}+1}$
g_M	5 mS/cm^2		
g_L	0.15 mS/cm^2	m_∞	$-\frac{(0.32v+17.28)\left(e^{\frac{v}{5}+\frac{27}{5}}-1\right)}{(0.28v+7.56)\left(e^{-\frac{v}{4}-\frac{27}{2}}-1\right)-(0.32v+17.28)\left(e^{\frac{v}{5}+\frac{27}{5}}-1\right)}$
E_M	-100 mV		
E_L	-67 mV	n_∞	$\frac{0.032v+1.664}{0.032v-0.5\left(e^{-\frac{v}{5}-\frac{52}{5}}-1\right)e^{-\frac{v}{40}-\frac{57}{40}}+1.664}$
E_K	-100 mV		
E_{Na}	50 mV		
B	1 mm^2		
E_R	0 mV		
a	0.003 μm^2/fg		
c	1 μF/cm^2		
T_{base}	295.15 K		
w_{tymp}	25.13 kHz		
k_s	91826.75 μm fg/ms^2		
τ_d	0.1 ms		
τ_z	1.19ms		
τ_w	100 ms		